Journal of Power Sources 248 (2014) 839–851

Contents lists available at ScienceDirect

Journal of Power Sources

journal homepage: www.elsevier.com/locate/jpowsour

Calendar and cycle life study of Li(NiMnCo)O_2-based 18650 lithium-ion batteries

Madeleine Ecker [a,c,*], Nerea Nieto [a,b], Stefan Käbitz [a,c], Johannes Schmalstieg [a,c], Holger Blanke [a,c], Alexander Warnecke [a,c], Dirk Uwe Sauer [a,c,d]

[a] Chair for Electrochemical Energy Conversion and Storage Systems, Institute for Power Electronics and Electrical Drives (ISEA), RWTH Aachen University, Jägerstrasse 17-19, 52066 Aachen, Germany
[b] IK4-IKERLAN, Miñano Menor, 01510 Alava, Spain
[c] Juelich Aachen Research Alliance, JARA-Energy, Germany
[d] Institute for Power Generation and Storage Systems (PGS) @ E.ON ERC, RWTH Aachen University, Germany

HIGHLIGHTS

- Extended accelerated aging tests on lithium-ion batteries including storage and cycling.
- Detailed analysis of influence of temperature and voltage on calendar aging.
- Detailed analysis of influence of cycle depth and SOC range on cycle aging.
- Influence of phase transition on calendar and cycle aging.
- Differential voltage analysis for identification of aging processes.

ARTICLE INFO

Article history:
Received 20 June 2013
Received in revised form
18 September 2013
Accepted 26 September 2013
Available online 11 October 2013

Keywords:
Calendar life
Cycle life
Aging
Lithium-ion
Nickel cobalt manganese
Phase transitions

ABSTRACT

An extensive set of accelerated aging tests has been carried out employing a Li-ion high energy 18650 system (2.05 Ah), negative electrode: carbon, positive electrode: Li(NiMnCo)O_2). It is manufactured by Sanyo, labeled UR18650E, and is a commercial off-the-shelf product. The tests comprise both calendar life tests at different ambient temperatures and constant cell voltages and cycle life tests operating the cells within several voltage ranges and levels using standard test profiles. In total, 73 cells have been tested. The calendar life test matrix especially investigates the influence of SOC on aging in detail, whereas the cycle life matrix focuses on a detailed analysis of the influence of cycle depth. The study shows significant impact of the staging behavior of the carbon electrode on cycle life. Furthermore a strong influence of the carbon potential on calendar aging has been detected. Observed relations between aging and the different influence factors as well as possible degradation mechanisms are discussed. Analysis of C/4 discharge voltage curves suggests that cycle aging results in different aging processes and changes in material properties compared to calendar aging. Cycling, especially with cycles crossing transitions between voltage plateaus of the carbon electrode seems to destroy the carbon structure.

1. Introduction

The increasing amount of lithium-ion batteries in the market of durable consumer and investment goods, like (hybrid) electric vehicles or temporary storage systems for renewable energy sources, requires a more sophisticated evaluation of battery lifetime in the special application. Aging has to be quantified as well as degradation mechanisms identified in order to develop operation strategies and business models. However, aging tests under real life conditions can be, depending on the application in consideration, time and cost intensive. Accelerated aging tests combined with lifetime simulations to extrapolate the aging results to real life conditions are needed to guarantee a lifetime prediction within the development cycle of a certain product.

* Corresponding author. Chair for Electrochemical Energy Conversion and Storage Systems, Institute for Power Electronics and Electrical Drives (ISEA), RWTH Aachen University, Jägerstrasse 17-19, 52066 Aachen, Germany. Tel./fax: +49 241 80 96943.
E-mail addresses: batteries@isea.rwth-aachen.de, er@isea.rwth-aachen.de (M. Ecker).

0378-7753/$ – see front matter © 2013 Elsevier B.V. All rights reserved.
http://dx.doi.org/10.1016/j.jpowsour.2013.09.143

A lack of knowledge of the occurring aging processes in lithium-ion batteries constricts the development of accurate lifetime prediction models. The understanding of calendar and cycle aging and especially of their interaction is of particular importance. In the past often one kind of aging has been addressed to for the cell under consideration, either calendar [1,2], or cycle aging [3–5]. Combined investigations have been accomplished considering Li(NiCo)O_2 [6,7] based batteries. Li(NiMnCo)O_2, being a promising candidate for automotive applications, has been considered in only few publications. In Refs. [8,9] calendar aging of Li(NiMnCo)O_2 based batteries has been discussed. In both works only few cycle life tests have been considered. Aging of Li(NiMnCo)O_2 based materials has been also investigated in Refs. [10–12], all concentrating on different influence factors on aging. Bloom et al. [10] for example compare calendar and cycle aging at different temperatures, without taking into account the influence of SOC or cycle depth. Dubarry et al. [11] study the cycle aging only for one aging condition (2 C cycling) focusing on the two stages in cycle aging. Finally, in Ref. [12] calendar as well as cycle aging tests have been performed at different temperatures and SOC, comparing different application profiles. However, the influence of cycle depth has not been considered.

Overall, the influence of cycle depth and SOC range of the cycle on aging has experienced little attention. Especially, there is little knowledge about mechanically induced aging. Studies on silicon materials show that volume changes in battery materials during operation do impact the mechanical stability of the materials [13,14]. Furthermore works on graphite electrodes reveal a relation between the staging behavior of the material and mechanical stresses [15–17]. However, this phenomenon is not completely understood. Also the impact on system level is rarely understood. The influence of cycle depth on aging has been examined by Wright et al. [6] for a $LiNi_{0.8}Co_{0.2}O_2$ system using a rather small amount of comparable test conditions. No reasonable model was found by the authors. So far the published works dealing with mechanically induced aging focus more on theoretical or simulation based calculation of mechanical stresses rather than dealing with experimental approaches. Physically based simulation results show that phase changes in the battery materials can lead to considerable mechanical stress [18]. Also results of Dokko et al. [19] indicate a relation between phase changes and particle fracture. A better understanding of the relation between phase changes in battery materials and cycle and calendar aging would imply a major benefit for the accuracy of lifetime predictions. Especially a fast detection of the conditions inducing the main part of stress in the cell via electrochemical measurements of the full cell are desirable.

In this work an extensive set of accelerated aging tests has been carried out employing a lithium-ion high energy 18650 system (2.05 Ah, negative electrode: carbon, positive electrode: Li(NiMnCo)O_2). Calendar as well as cycle aging tests have been conducted with a special focus on the influence of SOC and cycle depth on aging. In addition, the influence of temperature on calendar aging has been investigated. The aim is to provide correlations between aging and the various influence factors in order to provide input to lifetime prediction models. In a first step, different resistance and capacity definitions (e.g. resistances measured at different SOC or after different time spans) are compared to each other, in order to determine a representative parameter to analyze the aging results. In Sections 3.2 and 3.3 results of calendar and cycle aging tests are presented, respectively. Finally Section 3.4 draws a comparison between degradation during storage and cycling.

2. Experimental

For the aging investigation a high energy 18650 lithium-ion battery manufactured by Sanyo, labeled UR18650E has been used. The cell is designed for automotive application and has a capacity of 2.05 Ah. Voltage between 2.5 and 4.2 V is allowed by the manufacturer, with a nominal voltage of 3.6 V. The gravimetric energy density of the system is about 165 Wh kg^{-1}. The materials comprise carbon on the negative electrode and Li(NiMnCo)O_2 on the positive electrode. The cell specifications are summarized in Table 1.

Calendar aging tests were performed according to Table 2. The cells were stored at different ambient temperatures and voltages. During storage the cell voltage was kept constant (float condition) using an arbitrary power supply unit (HM8143 0–30 V/2 A). Temperature was regulated using ovens (Memmert UFE500 30 °C–250 °C). Main focus of the test matrix is the investigation of the impact of voltage on aging. The voltage was related to the state of charge (SOC) of a new cell using an open circuit voltage (OCV) measurement (Fig. 1) and was varied with high resolution in the test matrix. The voltage was adjusted starting from the discharged cell and charging the cell with a constant current and finally a constant voltage phase to the desired voltage level. For each test condition three cells were tested in order to prove the reproducibility of the measurement.

Similarly, cycling tests were performed following Table 3. Cells were cycled at 35 °C with 1 C current rate in different SOC ranges, where cycling devices (Digatron, ECO 10 A 0–6 V) have been employed. Temperature was controlled on cell level using temperature sensors on the cell surface. Temperature was regulated with climate chambers (Binder MK240 −40 °C to +180 °C and Binder MK53 −40 °C to +180 °C). For cycling one to three cells were tested at the same condition. The focus in this test matrix is on the influence of cycling depth (ΔDOD) as well as voltage level on aging. The adjustment of the voltage was performed with a constant current/constant voltage charging, again the OCV curve relates voltage and SOC. Starting from the mean voltage of a certain cycle, the cell is charged and discharged Ah-based to realize the cycling depth. ΔDOD always refers to the nominal capacity in this work, 10% ΔDOD means charge/discharge of 0.205 Ah from a certain voltage level. To prevent drifts in voltage caused by small errors in the Ah-calculation of the battery testing devices, cycling tests were balanced by readjusting the voltage after 100 cycles. Cycles touching SOC of 100 or 0% are adjusted according to the upper or lower voltage border, respectively. An exception is the cycle with cycling depth of 100%, which is cycled between the voltage borders without Ah-counting.

To access the aging of the cell, checkups were performed at begin of test, at end of test and in intervals of 7 weeks for calendar aging and 3 weeks for cycle aging in between. End of test is defined as the state when the actual capacity of the cell has decreased to 70% with respect to initial capacity or when the 2 s discharge resistance at 2 C rate has changed from its initial value by a factor of 3.

In each checkup the actual capacity and resistance of the cells were measured as well as C/4 discharge voltage curve measurements were performed. For selected cells also electrochemical

Table 1
Cell specification according to data sheet.

Nominal capacity	2.05 Ah
Material	Li(NiMnCo)O_2/carbon
Maximum continuous current	
Charge	1 C
Discharge	3 C
Allowed voltage range	2.5–4.2 V
Proposed voltage range	3.0–4.1 V
Temperature range	
Charge	0–40 °C
Discharge	−20–60 °C
Storage	−20–50 °C

Table 2
Calendar aging test matrix.

T [°C]	SOC [%]	0	10	20	30	50	60	70	80	85	90	95	100
	V [V]	3.331	3.494	3.578	3.626	3.699	3.782	3.869	3.964	4.018	4.072	4.117	4.162
50		X	X	X	X	X	X	X	X	X	X	X	X
40						X							
35						X							

impedance measurements were conducted. All checkups were performed at 35 °C. To ensure a cell temperature of 35 °C, equilibrium has been assumed when temperature has changed less than 1 K per hour.

The determination of the cells' capacity consists of a standard charge (1 C-rate constant current charge to 4.2 V, constant voltage charge at 4.2 V until the current has decreased below 0.02 C-rate), followed by a 1 C discharge to define the capacity. The charge and discharge resistances are determined using current pulses at different SOC (90–10% SOC in 10% steps). The SOC is adjusted Ah-based, referring to the nominal capacity at all times. I.e. to obtain 90% SOC of the cell, 0.205 Ah are discharged from a completely charged cell. At each SOC an 18 s 2 C-rate discharge pulse followed by a 40 s rest period and a 10 s 1 C-rate charge pulse also followed by a 40 s rest period is applied to the cell. Fig. 2 shows the voltage response to this pulse at begin of test. The generalized test protocol used for each constant current charge and discharge pulse, is based on the maximum current ratings specified by the manufacturer (Table 1). In particular, various discharge resistances (after 2 s, 10 s and 17 s), various charging resistances (2 s, 10 s), the discharge pulse power (after 2 s, 10 s and 17 s) and the charging pulse power (2 s, 10 s) are determined. In this work the 17 s discharge resistance R_{act} at 50% SOC is used for the aging analysis. The 17 s discharge resistance is calculated by the difference between the voltage before the pulse during the rest period and the one after 17 s of pulse duration, divided by the current (see Fig. 2). Likewise the 2 s and 10 s charge and discharge resistances are defined.

The OCV vs. SOC curve is only measured at begin and end of test. For the checkups a time-efficient alternative to assess changes in the phases of the material is to study the behavior of the C/4 discharge voltage curve. The cell is charged with the standard charge procedure described above and discharged at a constant, small current rate ($I = 0.25$ C-rate) to 2.5 V. After reaching 2.5 V the cell is again charged with the same current rate until reaching 4.2 V.

The impedance spectroscopic measurements serve to identify electrochemical properties of the system, such as effects related to the migration and diffusion processes within the cell. Impedance spectra are measured at 20, 50 and 80% SOC between 10 mHz and 5 kHz, using Electrochemical Impedance Spectroscopy devices (Digatron EIS-Meter, 0.3–3000 mΩ, 2 A AC (max), 0–20 V). In this work capacity fade, resistance increase and changes in the C/4 discharge voltage curve will be analyzed over aging. The results obtained by impedance spectroscopic measurements will be discussed in a separate paper.

To access the contribution of the single electrodes to the full cell behavior, an 18650 full cell has been disassembled under argon atmosphere. One side of the double-sided positive electrodes has been removed. Circular pieces with a diameter of 16 mm have been cut from the positive electrode using a punch. The $Li(NiMnCo)O_2$ has been inserted into a coin-cell together with a 16 mm piece of lithium, a separator and electrolyte consisting of 1 M $LiPF_6$ in an EC/EMC (1:1) solvent mixture. After a second formation cycle with 0.1 C between 3.0 V–4.2 V, the discharge curve has been recorded using 0.2 C. The negative electrode has not been used in half-cell measurements, because of strong flaking of the active material from the current collector.

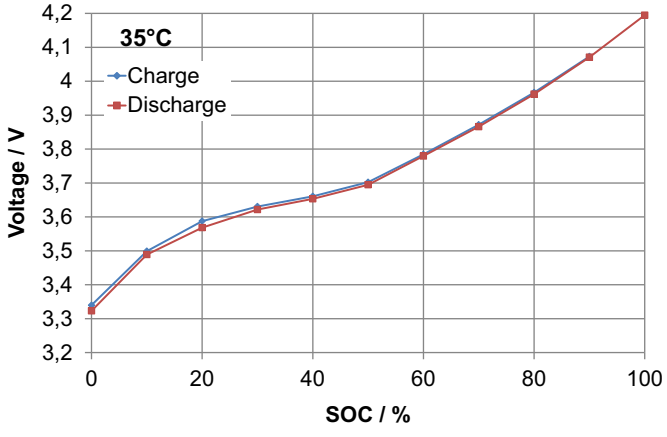

Fig. 1. Open circuit voltage over state of charge at 35 °C. SOC is related to the nominal capacity.

3. Results and discussion

3.1. Comparison of different resistance definitions

To find representative parameters to analyze aging results in the following, it is important to compare the different resistance definitions introduced in Section 2. The resistance has been calculated after different times of pulse duration, but also at different SOC of the battery.

Fig. 3 compares the evolution of resistances measured after different pulse durations for the 3 cells aged by storage conditions at 50 °C and 90% SOC. Fig. 3a) depicts the resistances measured at 30% SOC and Fig. 3b) the ones measured at 70% SOC. In Fig. 3a) all resistances show almost the same aging behavior. Also in Fig. 3b) most of the resistances show similar aging behavior, excepting the 2 s charge and discharge resistances, which both have a slightly higher aging rate. Results from impedance spectroscopy in Fig. 4 show, that the diffusion dominated part of the spectra (diffusion branch) starts for 20% SOC, 50% SOC and 80% SOC at frequencies of 1.5 Hz, 6.7 Hz and 6.6 Hz, respectively. This means that all resistances measured after pulse durations >0.67 s reflect the ohmic and the charge transfer processes of the cell and therefore include the same degradation mechanisms. In some cases it may be that after 2 s of pulse duration there are still some parts of charge transfer not included in the measurement, leading to the observed change in aging rate. The two figures are chosen exemplarily, as the two cases show the behavior of the majority of the tested cells. In most cases the resistances determined after different pulse duration show similar aging trends. The deviations for cells aged during cycling are slightly higher than for the stored cells. While the 2 s charge and discharge resistances deviate from the other resistances for some stored cells. In the case of the cycled cells it is more the charge resistances that deviate from the discharge resistances.

Table 3
Cycle aging test matrix.

T [°C]	35					
C-rate	1					
ΔDOD [%]	100	80	50	20	10	0 5
SOC-range [%]	0–100	10–90	50–100	80–100	90–100	87.5–92.5
			25–75	65–85	85–95	72.5–77.5
			0–50	40–60	70–80	47.5–52.5
				15–35	45–55	22.5–27.5
				0–20	20–30	
					5–15	

To investigate how the aging rate of the resistance depends on the SOC the resistance is measured at, Fig. 5 shows the 17 s discharge resistance measured at 50% SOC over the 17 s discharge resistance measured at 90% SOC for different checkup times. Fig. 5a) depicts this comparison for all calendar aging tests conducted at 50 °C and Fig. 5b) for the cycling tests. It can be concluded, that for the calendar as well as for the cycle aging tests the aging rate of the resistance is not significantly depending on the SOC, the resistance is measured at. This makes an implementation of a state of health prediction in a battery management system easier. Anyway, there are little deviations, especially for cells in a later stage of life, where the resistance measured at 50% SOC ages faster than the one measured at 90% SOC. This effect is more pronounced for lower SOC. A reason therefore is certainly that the voltage where the measurement is conducted at shifts over aging. This is due to the fact, that the SOC is always adjusted Ah-based referring to the nominal capacity in this experimental setup.

Based on the finding that the different resistance definitions show similar trends during aging, the 17 s discharge resistance measured at 50% SOC as well as the capacity determined using a 1 C discharge rate will be considered as representative parameters for the following analysis of the experimental data, as mentioned in Section 2. As mentioned before, this analysis is also important for the development of aging models and battery management systems. Especially in battery management systems, the actual state of the system, for example the actual power capability or the state of health, needs to be estimated in each moment. During operation the SOC, temperature and current rate usually change. Therefore it is important to know, whether only one function is needed to calculate the aging of the resistance, or whether different aging rates apply to resistances determined at different conditions. Deeper investigations on this topic have been conducted by Ref. [20].

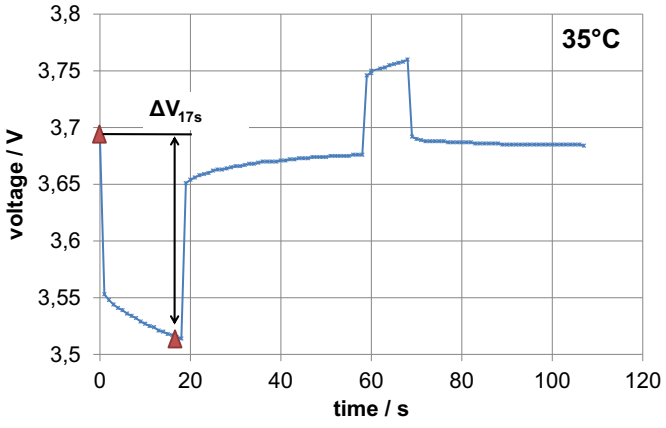

Fig. 2. Voltage response of the cell to the high pulse power characterization profile at 50% SOC and 35 °C. The red triangles mark the voltage values used for calculation of the 17 s discharge resistance. (For interpretation of the references to color in this figure legend, the reader is referred to the web version of this article.)

3.2. Calendar aging tests

During calendar aging tests cells were stored at different SOC and temperatures. Fig. 6 shows capacity fade and resistance increase for cells stored at 50 °C at different SOC. As expected, cells stored at lower SOC exhibit a longer lifetime. Especially cells stored at 100% SOC show a much faster degradation compared to other SOC. These cells only reach a lifetime of 107 days at 50 °C until capacity reaches 80% of the initial value (linear interpolation). At this time the resistance increased by a factor of 1.3. For comparison, cells stored at 95% SOC reach 288 days until end of life (linear interpolation), whereas a cell stored at 0% SOC has an extrapolated lifetime of about 4 years (linear extrapolation of the last three measured data points). At moderate temperatures, e.g. 40 °C, cells stored at 50% SOC last for about 3 years (linear extrapolation of the last three measured data points) before reaching end of capacity lifetime. Capacity fade and resistance increase for cells stored at different temperatures at 50% SOC are shown in Fig. 7. Higher temperature leads to faster aging concerning capacity as well as resistance. Fig. 7 also displays the evolution of the single cells stored at the same conditions. The capacity data exhibit very low scattering, whereas a spread can be observed in the resistance data.

Most aging curves show a nearly linear aging behavior. Theory of film formation on electrodes [21,22] states, that a solid electrolyte interface (SEI) film growth on the negative electrode proceeds with a square root of time dependency, due to passivation of the negative electrode surface. On the positive electrode also surface films

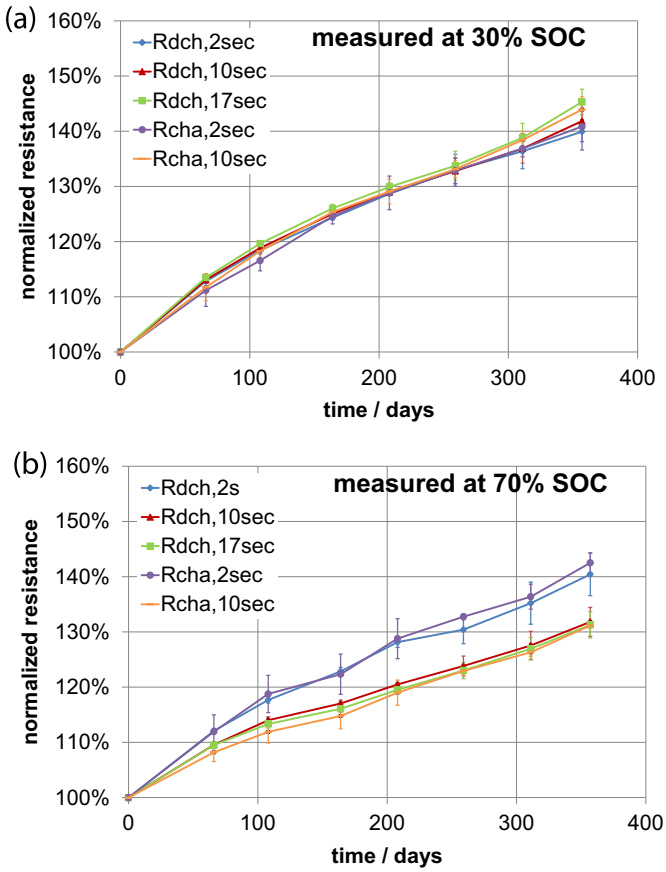

Fig. 3. Comparison of resistances determined after different pulse duration over time. Values for cells stored at 50 °C and 90% SOC normalized to the initial value are displayed. (a) Shows the resistances measured at 30% SOC, (b) at 70% SOC. All resistance measurements were conducted at 35 °C. The mean values of 3 cells are shown together with standard deviation.

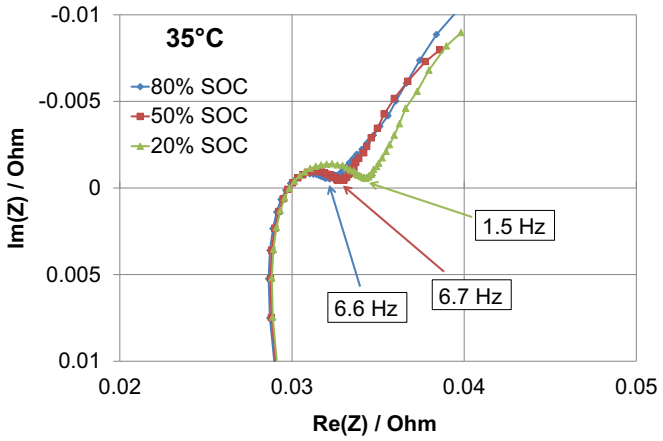

Fig. 4. Impedance spectra of a new cell measured at 35 °C at different SOC. The arrows indicate the frequencies of the knee of the spectra, where diffusion starts to dominate.

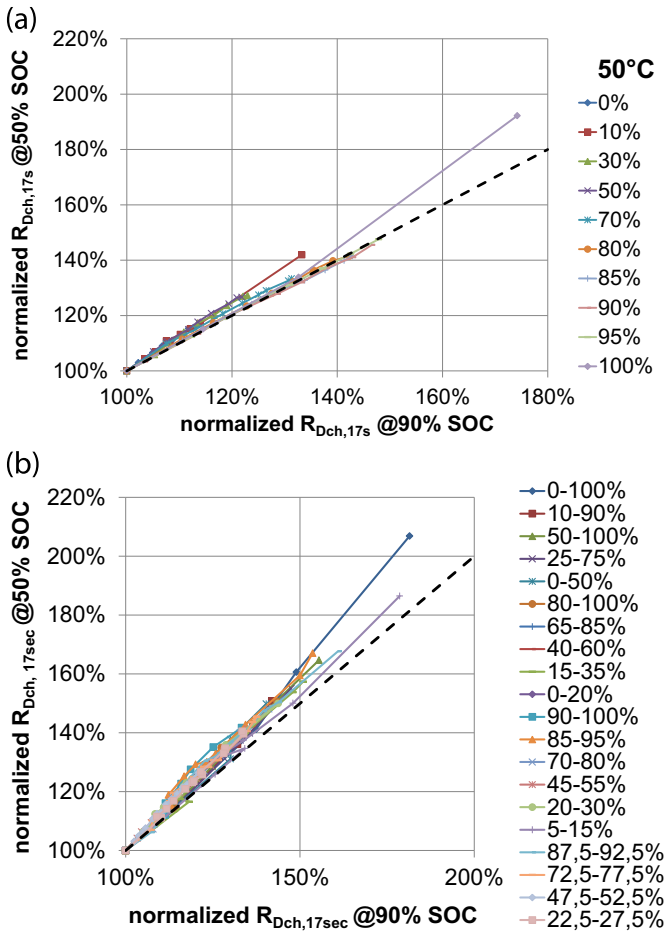

Fig. 5. 17 s discharge resistance normalized to the initial value measured at 50% SOC over 17 s discharge resistance normalized to the initial value measured at 90% SOC for different checkup times. All resistances are measured at 35 °C. In (a) cells stored at 50 °C at different SOC are depicted. The mean values of cells stored at the same condition are shown. (b) Illustrates cells cycled in different SOC ranges at 35 °C. Here the values of single cells are shown, as the checkups of cells cycled at the same conditions were not conducted in exactly same time intervals. The black slashed line indicates equality of the two resistances.

have been detected. Compared to the SEI, positive electrode surface films have been demonstrated to exhibit no passivation character, but electrolyte is transported continuously to the positive electrode surface. That is the reason why positive electrode surface films have been named 'solid permeable interface' (SPI) [23]. The non-passivation character of positive electrode surface films suggests a more linear growth with time. During storage the main aging processes are expected to be film formation on the negative electrode as well as on the positive electrode side, however SEI formation on the negative electrode is presumed to be the dominant effect [22,24–26]. As growth of film is directly related to capacity loss (due to loss of active lithium) and to resistance increase (due to increase in film layer thickness), a square root of time evolution of capacity fade and resistance increase was expected in the storage tests due to SEI formation. In contrast to theory of SEI formation the evolution of capacity and resistance during storage in this test especially at low SOC shows a more linear behavior. Only slight square root tendencies can be seen, indicating additional aging mechanisms beside SEI formation. One explanation could be a strong contribution of positive electrode surface film formation. But later discussion shows that the negative electrode potential has strong impact on calendar aging of the cell (Section 3.2.2). Another possibility would be a capacity increasing effect as proposed in Ref. [9] that superimposes SEI formation.

3.2.1. Influence of temperature

To analyze the influence of temperature on aging, Arrhenius analysis for capacity fade and resistance increase of cells stored at 50% SOC is conducted. The Arrhenius equation describes the dependency of the reaction rate of a chemical reaction on temperature:

$$A = A_0 \cdot \exp\left(-\frac{E_a}{RT}\right)$$

where A_0 is a pre-exponential factor, R the universal gas constant, T the temperature in Kelvin and E_a the activation energy in kJ mol^{-1}. This analysis provides the baseline to study thermally activated processes in degradation.

Fig. 8 displays Arrhenius plots for capacity loss and resistance increase of cells stored at 50% SOC. Since the checkup intervals for the cells stored at 50 °C have been slightly different from the tests conducted at 35 °C and 40 °C, the values have been linearly interpolated to comparable storage times. Logarithm of the two parameters is plotted vs. the inverse temperature. For capacity loss clearly a linear relation can be observed. The resistance deviates from the linear behavior, which can be due to the scattering in the resistance measurement displayed in Fig. 7. Especially between resistance increase of the 35 °C and 40 °C cells only small dependency on temperature can be derived due to the scattering in the data.

Capacity fade activation energy has been derived from the slope of the observed linear relation. For fitting a linear regression is conducted considering three cells for each test condition. The fitting results are shown in Table 4. The correlation coefficients demonstrate clearly the linear relation. Fig. 9 also displays the resulting activation energies derived from capacity loss of cells stored at 50% SOC over storage time. The activation energies range from 47 to 60 kJ mol^{-1}, which is similar to the activation energies derived by Liaw et al. [27] in the range of 50 kJ mol^{-1} in the initial stage of aging. Fig. 9 shows no clear trend of activation energies over time. This constant value of activation energy could indicate a main degradation process that dominates during the different stages of aging.

3.2.2. Influence of voltage

Fig. 10 investigates the influence of voltage level on calendar aging in more detail. Normalized capacity as well as normalized

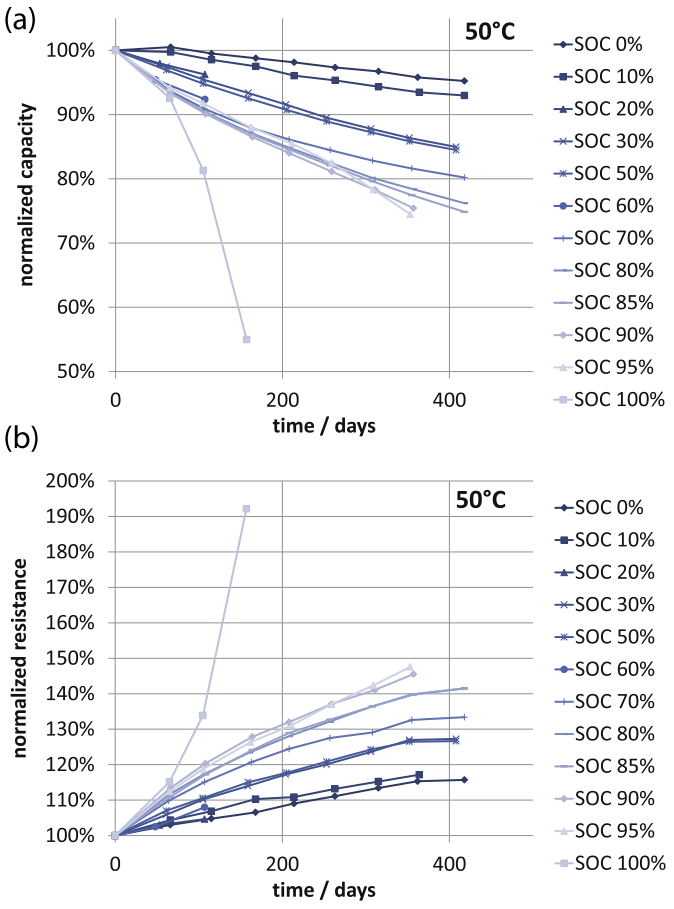

Fig. 6. (a) Normalized capacity vs. time and (b) normalized resistance vs. time for cells stored at 50 °C and different SOC. The mean values of 3 cells are shown, respectively.

resistance are shown vs. voltage for different storage times for cells stored at 50 °C. It has been already outlined in Section 3.2, that degradation proceeds faster at high voltage levels. Especially at 100% SOC the cells age disproportionally faster compared to other SOC, probably due to electrochemical instability of the electrolyte in this potential window. Also mentionable is the behavior of cells stored at 95% SOC. At least up to 260 days of storage they seem to age slower compared to cells stored at 80%–90% SOC. Further work on post-mortem analysis of these cells could shed light on the nature of this behavior. A high change in degradation rate can be observed between cells stored at 10% and 30% SOC as well as between 50% and 70% SOC. Especially the cells stored at 30% and 50% SOC show a quite similar aging behavior. This effect can also be observed in a more pronounced way in Fig. 6 in which 4 groups of curves can be clearly distinguished. There seems to be a change in material properties of the negative or positive electrode above 50% and below 30% SOC. Both, capacity and resistance show the trends discussed above, even though there is more scatter in the resistance data.

To study the observed effect in more detail, Fig. 11 outlines a differential voltage analysis of a charge and discharge curve of a new cell. Fig. 11a) shows voltage (right axis) as well as the differential voltage dV/dSOC (left axis) vs. SOC for an 18650 full cell. Clearly two peaks in the differential voltage can be outlined between 10% and 30% SOC and between 60% and 70% SOC. Only small changes in voltage can be observed between 30% and 60% SOC. Fig. 11b) shows voltage (right axis) as well as the differential voltage dV/dSOC (left axis) vs. SOC of a discharge for a Li(NiMnCo)O_2 half-cell (coin cell Li(NiMnCo)O_2/lithium). The graph indicates no peaks in the differential voltage curve of positive electrode, except at a potential of 3 V vs. Li. However, the peaks in the full cell discharge curve are observed at around 3.5 V, indicating, that the Li(NiMnCo)O_2 material is not cycled down to 3 V in the full cell. The absence of peaks in the differential voltage curve of the positive electrode in the used voltage range suggests that the observed two peaks in the full cell curve are due to staging phenomena in the negative electrode material. Based on results from electrochemical and XRD measurements, it is widely accepted that the intercalation of Li^+ into graphite can be described by a staging model [28–30]. According to this staging model the plateaus in the open circuit voltage of graphite electrodes correspond to two-phase regions with two coexisting phases. Therefore it can be concluded that peaks in the differential voltage curve of the full cell result from transitions between two-phase regions in the negative electrode, including a voltage plateau of the negative electrode between 30% and 60% SOC. This voltage plateau at the negative electrode clearly correlates with the observed degradation behavior in this SOC range. As the potential of the negative electrode does not change in this range, the cells show nearly identical degradation behavior. During transitions between the voltage plateaus (10%–30% SOC and 60%–70% SOC) in contrast negative electrode potential changes which is accompanied by high changes in the degradation rate during storage of cells between these voltage levels. The result leads to the conclusion that negative electrode potential influences strongly the degradation behavior of the total battery.

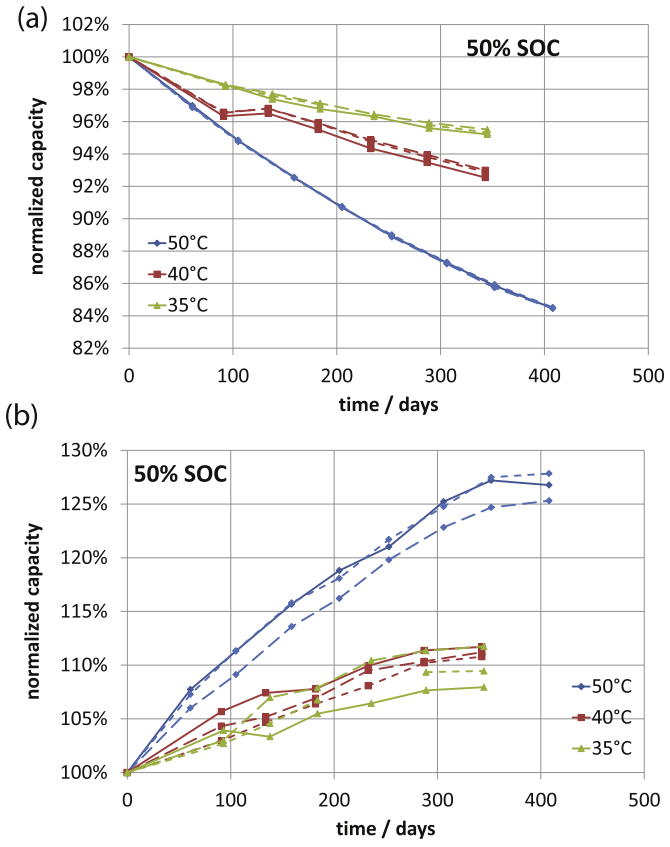

Fig. 7. (a) Normalized capacity vs. time and (b) normalized resistance vs. time for cells stored at 50% SOC and different temperatures. The results of single cells are shown, respectively. The different colors (or markers) indicate the different temperatures, whereas the three different line types (sometimes nearly on the same curve and therefore difficult to separate) describe the different cells tested under same condition. (For interpretation of the references to color in this figure legend, the reader is referred to the web version of this article.)

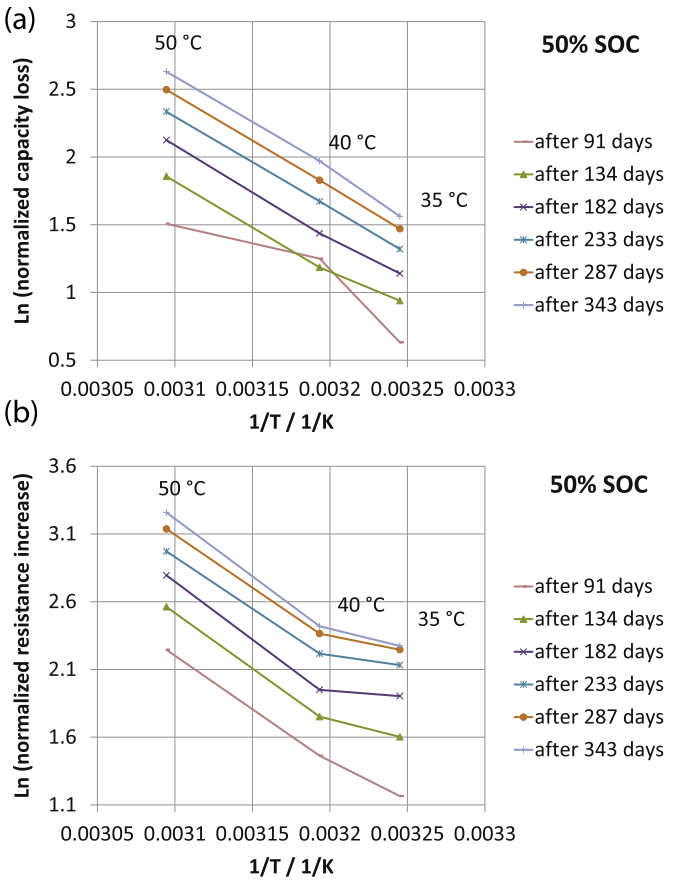

Fig. 8. (a) Logarithm of normalized capacity loss and (b) logarithm of normalized resistance increase vs. inverse of temperature for different state of health for cells stored at 50% SOC. The mean values of three cells are shown.

3.3. Cycling aging tests

During the cycle aging tests the cells were cycled with a 1 C rate keeping the cell temperature at 35 °C. This is a modest user profile, operating the battery within temperature as well as current limits given by the manufacturer. Fig. 12 shows capacity fade and resistance increase for cells cycled at different cycle depths around an average SOC of 50%. Cells that performed 100% cycles showed the fastest degradation, allowing in average 440 equivalent full cycles until capacity reaches 80% of the initial value (linear interpolation). At this time the resistance increased by a factor of 1.8. The cell with the lowest degradation rate was the one cycled between 47.5 and 52.5% SOC, allowing 8500 equivalent full cycles (linear extrapolation using the first and the last data point). In contrast to the calendar aging tests, the time evolution of capacity and resistance during cycling shows in most cases a slight square root dependency on time. Reaching a certain stage in lifetime, the cells die suddenly

Table 4
Activation energies derived from Arrhenius analysis for capacity loss after different storage durations at 50% SOC. R^2 gives the correlation coefficient of the fit.

Days	Activation energy [kJ mol^{-1}]	R^2
91	47.97	0.814
134	53.75	0.989
182	56.68	0.992
233	51.93	0.937
287	57.91	0.996
343	59.71	0.994

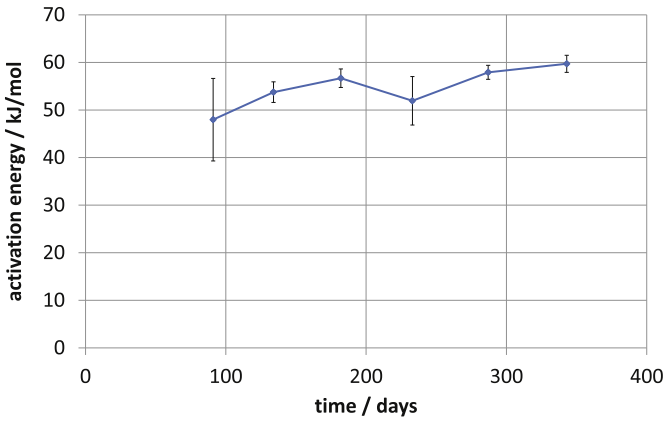

Fig. 9. Activation energy for capacity loss vs. storage time. Cells were stored at 50% SOC.

within only a few cycles. The point in lifetime of this sudden cell death is quite different even for cells aged under the same conditions. Fig. 12 shows this effect for the cells cycled between 0 and 100%, 10–90% and 25–75% SOC, where more than one cell at each condition has been tested. One of the cells cycled between 0 and 100% SOC for example dies suddenly between 760 and 950 equivalent full cycles, the other one between 250 and 500 and the third between 500 and 751. This is a large spread and a big challenge for lifetime predictions. It is remarkable that usually sudden death takes place, when the cells reach about 150% of their initial

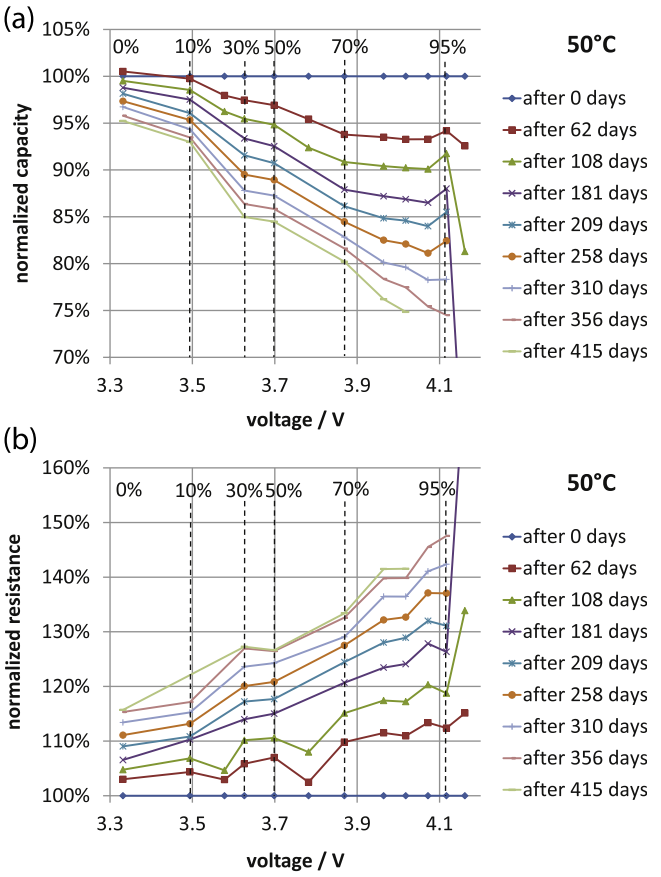

Fig. 10. (a) Normalized capacity vs. voltage and (b) normalized resistance vs. voltage for different state of health for cells stored at 50 °C. On top the corresponding SOC is displayed. The mean values of three cells are shown.

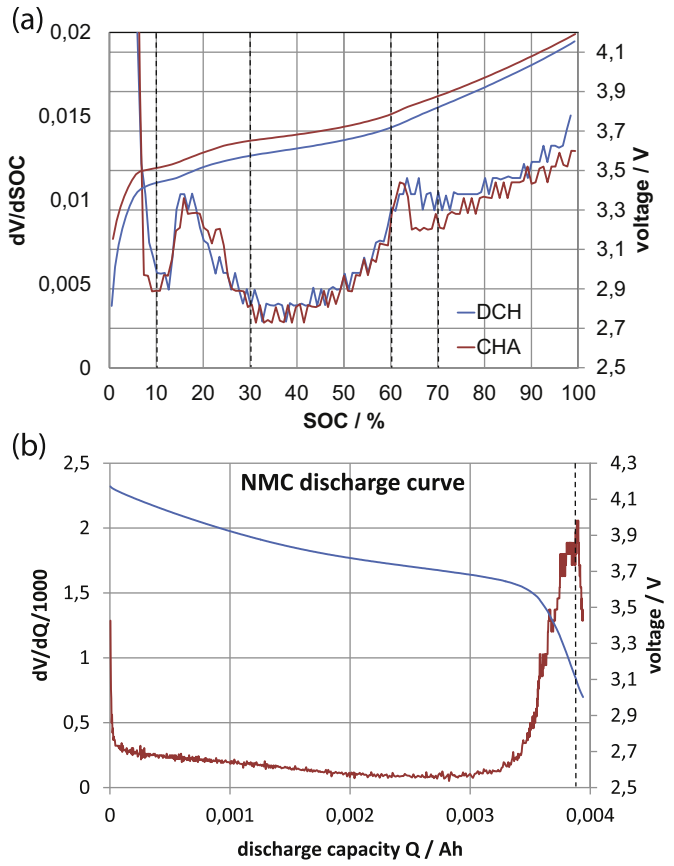

Fig. 11. (a) differential voltage d*V*/dSOC (left axis) and voltage (right axis) vs. SOC for an 18650 full cell. A charge curve (red) as well as a discharge curve (blue) are shown. Both are conducted with 0.25 C at 35 °C. The dashed lines divide the curve into two-phase regions and regions with transitions between voltage plateaus. Data from a single cell at begin of test is shown. (b) differential voltage d*V*/d*Q* (left axis) and voltage (right axis) vs. discharge capacity *Q* for a Li(NiMnCo)O_2 half-cell (coin cell). A discharge curve between 4.2 and 3.0 V with 0.2 C at 25 °C is shown for a single cell at begin of test. Voltage is measured against lithium. (For interpretation of the references to color in this figure legend, the reader is referred to the web version of this article.)

resistance and most of them have capacities of about 80% of the initial one. This supports the theory of Broussely et al. [24] that the sudden change of the slope in the aging curve is due to lithium-plating. Lithium-plating sets in, when the resistance of the negative electrode reaches a certain amount, where the negative electrode potential drops below 0 V vs. lithium during charging. According to Ref. [24] this polarization is mainly due to a reduced active surface area at the negative electrode caused by deposition of SEI products and is further amplified by deposition of products due to lithium-plating. Anyway, the data do not give further hints to the origin of the sudden death, which makes it difficult to identify lithium-plating as the only reason for the break down.

The extrapolated lifetimes above have to be regarded carefully, as the linear extrapolations do not take into account the sudden deaths discussed above. Extrapolations have been conducted to 80% of initial capacity. As most cells do not fail before reaching 80% of initial capacity, the values can be regarded as a rough estimation.

3.3.1. *Influence of cycle depth and voltage level*

Fig. 12 already indicates that the cycle depth has great impact on cell degradation. The deeper the cycle depth is, the faster proceeds aging. The influence of cycle depth on aging has been tried to examine by Wright et al. [6] for a $LiNi_{0.8}Co_{0.2}O_2$ material. No reasonable model was found by the authors. Investigating a $LiFePO_4$ material. Wang et al. [3] even found no influence of cycle depth on aging. Fig. 13 depicts the influence of cycle depth on aging for the Li(NiMnCo)O_2 material considered in this work. Capacity fade and resistance increase over cycle depth for cells cycled in different voltage levels after reaching 750 equivalent full cycles are shown. The data reveal a clear dependency of aging on cycle depth; however the proper mathematical description is not clear. From the results a linear dependency on cycle depth for capacity fade, as well as for resistance increase is suggested.

For other technologies, e.g. lead-acid batteries [31], SN or Wöhler curves are commonly used to describe the influence of cycle depth on lifetime. Wöhler curves were originally used in German railway engineering to determine the lifetime of railway components before failure in dependence on mechanical event or stresses. In battery technology, usually the number of equivalent full cycles until end of life of the battery is plotted vs. cycle depth. In Fig. 14 Wöhler curves for cells cycled with 1 C at 35 °C around different average voltages are shown using a lifetime criterion where the capacity reaches 80% of the initial value. In some cases linear interpolation has been applied to calculate the number of equivalent full cycles, in other cases extrapolations have been necessary. Extrapolations have been conducted in a linear way using the first and the last data point, which seems to be reasonable looking at the very slight square root (more linear) dependencies of the cycling tests on time. 80% of capacity has been chosen in order to prevent false conclusions due to sudden death. The Wöhler curve shown in Fig. 14 is in principle a 3 dimensional Wöhler curve. The

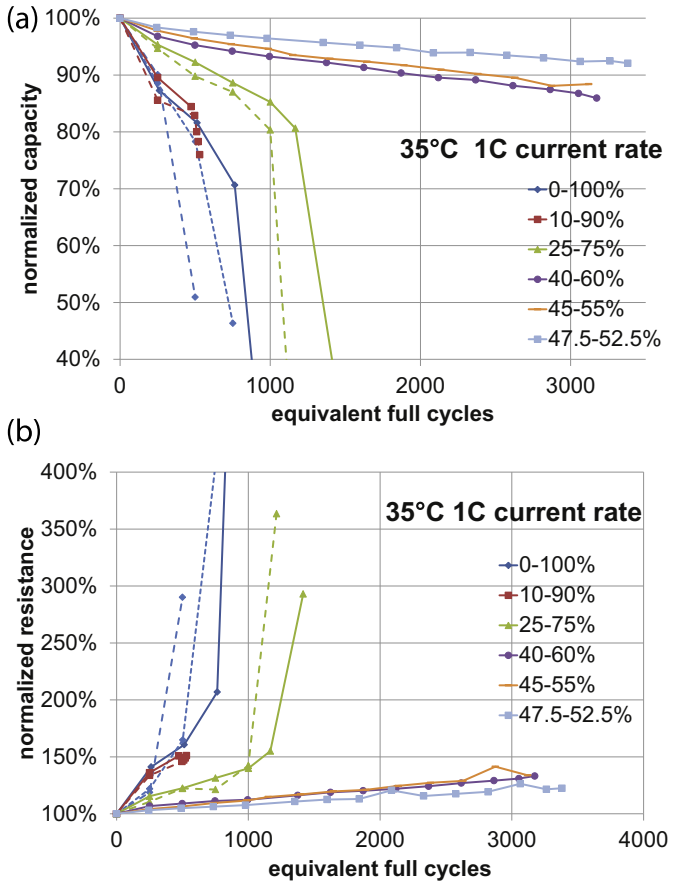

Fig. 12. (a) Normalized capacity vs. equivalent full cycles and (b) normalized resistance vs. equivalent full cycles for cells cycled with 1 C at a cell temperature of 35 °C. Different cycle depths around a mean SOC of 50% are compared. Data of the single cells is shown.

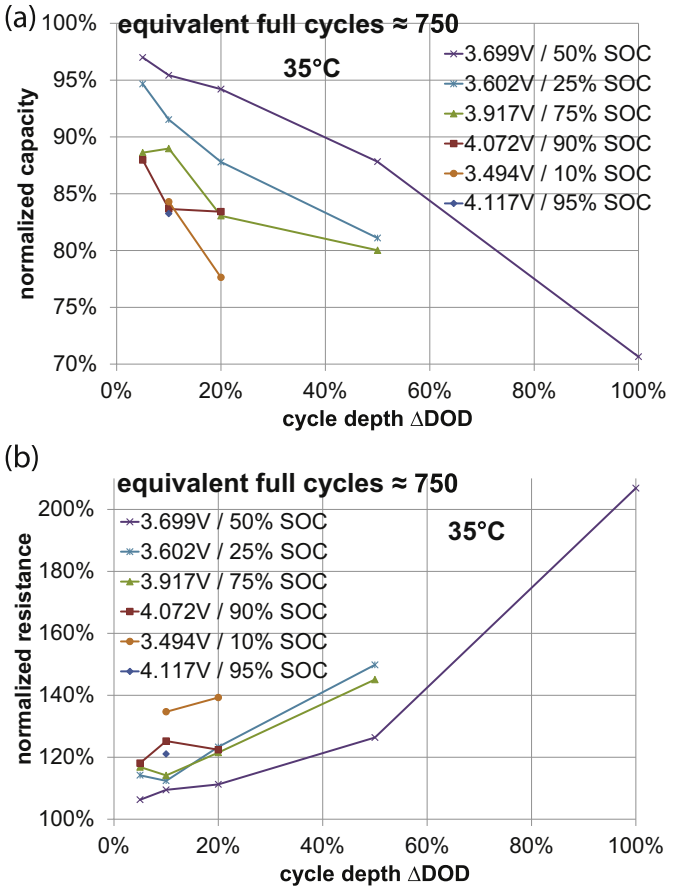

Fig. 13. (a) Capacity normalized to the initial value and (b) resistance normalized to the initial value after 750 equivalent full cycles vs. cycle depth. A comparison of cells cycled with 1 C at 35 °C around different average voltages is shown. Mean values are shown.

number of cycles depends on cycle depth as well as on the average voltage the battery is cycled around. In theory the Wöhler curve is even 5 dimensional, as the number of cycles additionally depends on temperature and current rate. As the influence of current rate and temperature on cycle aging has not been investigated in this work, only a 3 dimensional Wöhler curve is displayed. In comparison to the illustration in Fig. 13 which shows a linear dependency

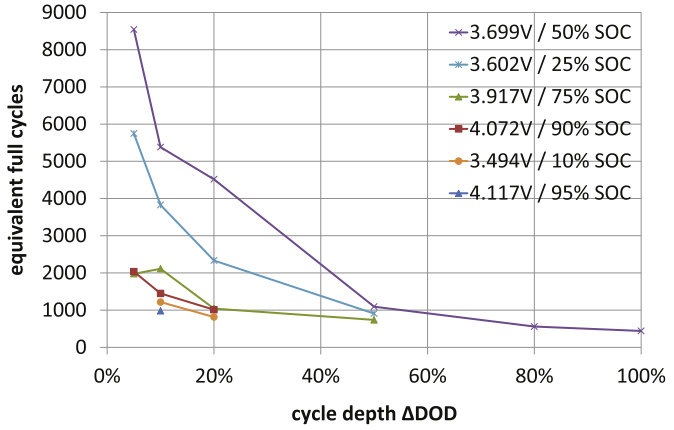

Fig. 14. Wöhler curves for cells cycled with 1 C at 35 °C around different average voltages. Number of equivalent full cycles until capacity reaches 80% of the initial value vs. cycle depth is shown.

of capacity fade on cycle depth, the number of cycles in Fig. 14 shows a non-linear dependency. This is due to the reciprocal relation between capacity fade and number of equivalent full cycles until end of life. Often exponential dependency is assumed for a Wöhler curve, but the data for the cell used in this work reveal a 1/ΔDOD relation.

Fig. 15 shows capacity fade and resistance increase for cells cycled with a cycle depth of 10% around different average SOC. It can be noticed, that especially cells cycled in high and low SOC ranges show the fastest degradation. A minimum in aging can be detected for the cells cycled around 50% SOC. Similar behavior can be seen for other cycle depths. Fig. 16 depicts the influence of voltage level on aging for cells cycled with different cycle depths. Capacity fade and resistance increase over average voltage after reaching 750 equivalent full cycles are shown for different cells. The analysis clearly indicates a 'U-shape' dependency of degradation on voltage level the cell is cycled around with a minimum around 50% SOC for capacity fade as well as resistance increase. For battery management this means for this cell, that avoiding very high and very low SOC during cycling helps prolonging lifetime. In contrast, as shown in Section 3.2.2 storing the battery at low SOC can help to prolong lifetime as well.

The data also indicate a relation between cycling and the staging behavior of the graphite material, similar to the observations discussed for calendar aging in Section 3.2.2. Especially cells cycled in SOC ranges crossing transitions between voltage plateaus of the negative electrode seem to age faster. In Fig. 11 transitions between the voltage plateaus in the graphite material have been outlined in

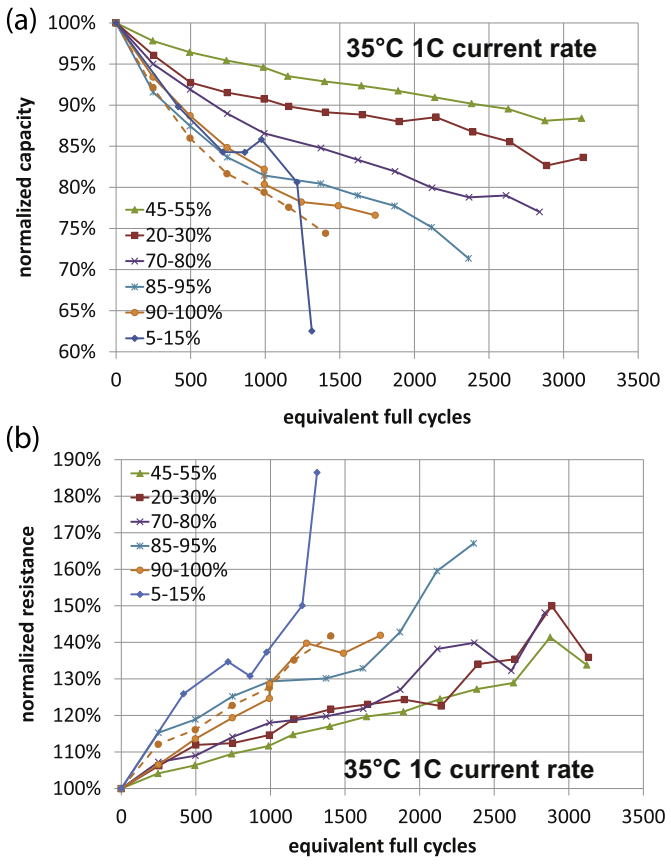

Fig. 15. (a) Normalized capacity vs. equivalent full cycles and (b) normalized resistance vs. equivalent full cycles for cells cycled with 1 C at a cell temperature of 35 °C. Cells cycled around different mean SOC with a cycle depth of 10% are compared. Data of the single cells is shown.

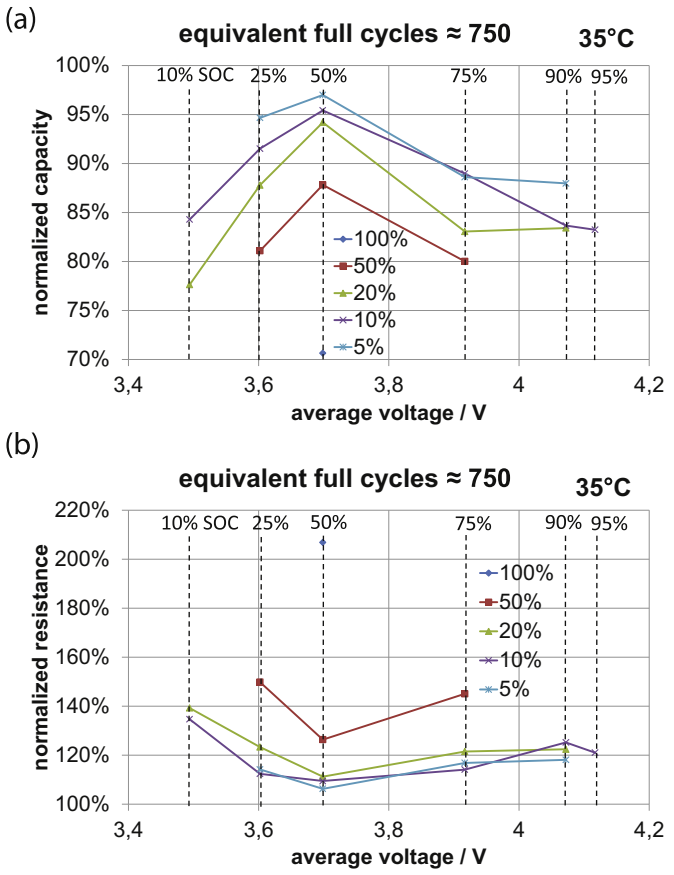

Fig. 16. (a) Capacity normalized to the initial value and (b) resistance normalized to the initial value after 750 equivalent full cycles vs. average voltage. A comparison of cells cycled with 1 C at 35 °C with different cycle depths is shown. Mean values are shown.

SOC rages between 10% and 30% SOC and 60% and 70% SOC with peaks at 17% SOC and 64% SOC, respectively. The staging features of the negative electrode are usually accompanied by changes in material properties. Especially lattice parameters change depending on the predominant phases [28], leading to material expansion and contraction and therefore to mechanical stress. Fig. 17 shows the influence of the staging behavior on cells cycled with a cycle depth of 20% SOC. Capacity fade over average voltage after reaching 750 equivalent full cycles is shown for cells with depth of discharge of 20% in (a), whereas (b) displays the differential voltage curve, showing the location of the transitions between the voltage plateaus as well as the SOC ranges the considered cells are cycled at. It has to be kept in mind, that the damage due to cycling/mechanical stress is superimposed by the damage caused by the voltage level itself, discussed in Section 3.2.2. The higher the voltage, the faster is the aging. Analyzing the different test conditions, it can be seen, that the cells cycled between 0% and 20% SOC and 15% and 35% SOC both cross the maximum of the transition between the plateaus at 17% SOC. In both cases, in spite of the low voltage level, the cells show fast degradation. The cell cycled in the two-phase region (voltage plateau) between 40% and 60% SOC on the other hand, shows the lowest degradation. The voltage transition at 64% SOC seems to have smaller impact on aging. The cell cycled between 65% and 85% SOC cross the transition at 64% SOC, but shows slower aging compared to the 0% and 20% cell despite the higher voltage level. Compared to the cell cycled between 65% and 85% SOC, the cell cycled between 80% and 100% SOC does not cross the voltage transition at 64% SOC. Due to the higher voltage level, the cell cycled between 80% and 100% SOC is supposed to age faster. This is not the case, due to the additional mechanical stress of the 65% and 85% cell probably caused by the transition. The observation leads to the speculations, that cycles in SOC ranges that cross transitions between voltage plateaus of the negative electrode, have a significant negative impact on cycle aging, due to higher mechanical stresses.

Also tests conducted at lower depth of discharge reveal similar correlations. But the above conclusions are more difficult to draw considering data of cells cycled at high SOC with lower cycle depth, as there is a strong superposition of calendar aging in the high SOC range. Therefore the results derived by the tests at 20% depth of discharge only give hints to the relation discussed here and the effect has to be studied in more detail, using additional test conditions.

Due to the system oriented approach of this work no conclusion could be drawn on the predominant stages of the graphite in the SOC range of the full cell. In order to draw a direct correlation between the observed effects and the lattice parameters half-cell measurements of the negative electrode as well as XRD measurements would be needed.

3.4. Comparison between calendar and cycle aging

Fig. 18 draws a comparison between calendar and cycle aging at 35 °C. Cells cycled with 1 C with three different depths of

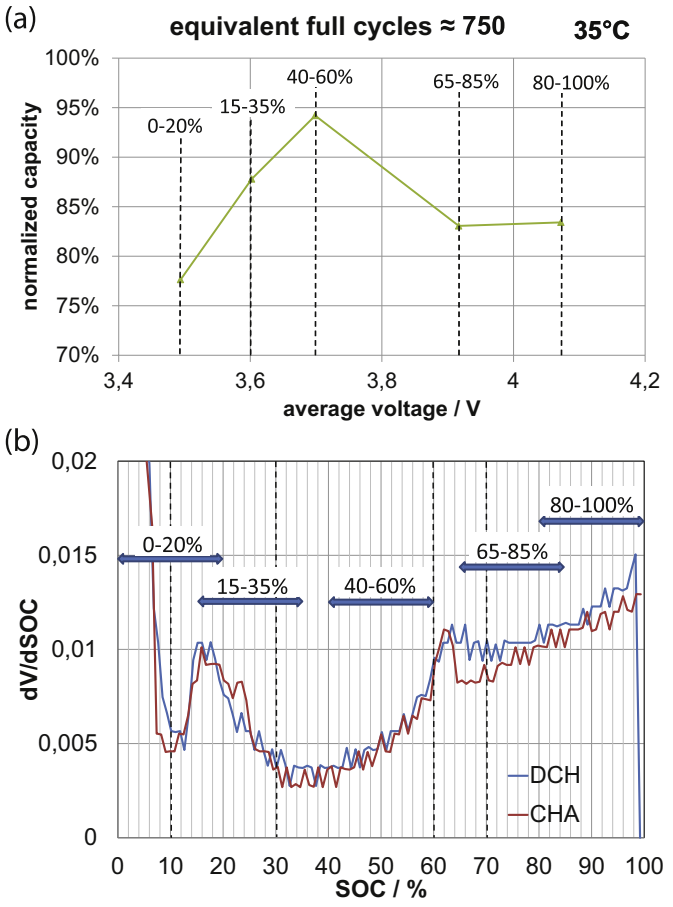

Fig. 17. (a) Capacity normalized to the initial value after 750 equivalent full cycles vs. average voltage. Mean values of cells cycled with 1 C at 35 °C and cycle depths of 20% are shown. (b) Differential voltage dV/dSOC vs. SOC for a charge (red) as well as a discharge curve (blue) for a new cell. Both are conducted with 0.25 C at 35 °C. The dashed lines divide the curve into two-phase regions and regions with transitions between voltage plateaus. The arrows indicate the SOC ranges of the cells cycled with cycle depth of 20%. (For interpretation of the references to color in this figure legend, the reader is referred to the web version of this article.)

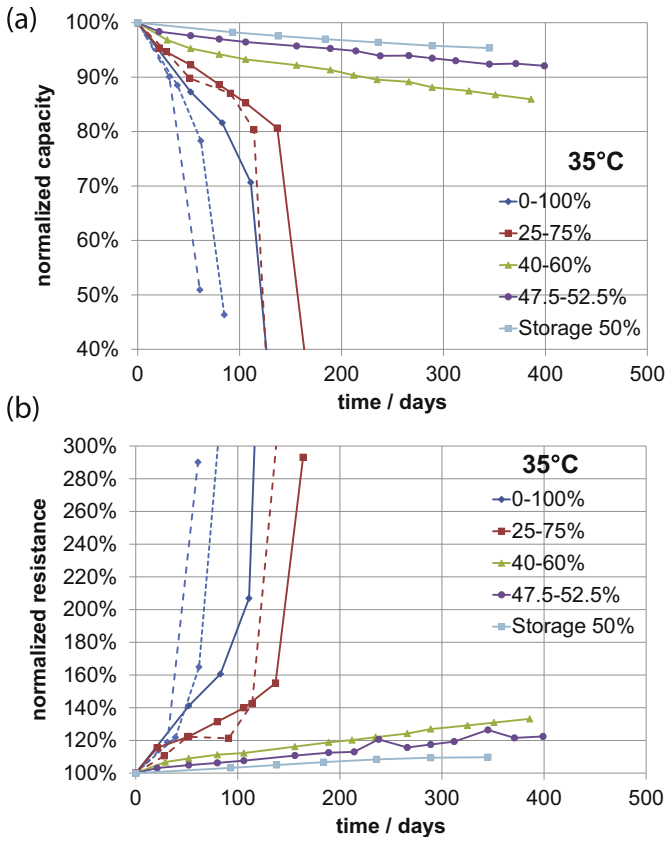

Fig. 18. Comparison between cycling and storage. (a) Normalized capacity vs. time and (b) normalized resistance vs. time for cells cycled with 1 C at a cell temperature of 35 °C and cells stored at 50% SOC at 35 °C. Different cycling depths around a mean SOC of 50% are compared. For cycling tests data of the single cells are shown, for the storage test average values are displayed. 400 days correspond more or less to 3200 equivalent full cycles.

discharge around a mean SOC of 50% are compared with cells stored at 50% SOC. Data for capacity fade as well as resistance increase display, that cycling adds additional degradation, or accelerates aging with respect to storage, even if only cycles with small cycle depth are applied. It has to be stressed at this point, that this finding cannot be generalized and the relation between calendar and cycle aging can be very different for other batteries under consideration, even if the basic electrode chemistry is the same. Looking at Li(NiMnCo)O_2-based high power pouch cell, Ecker et al. [8] for example, found that at least for the resistance, cycling prolongs lifetime. In their investigations of cells at 40 °C, resistance increased much faster during storage than under operation. Additionally, it is not clear, how the cells behave at higher temperatures than 35 °C. One could imagine a change in impact of calendar and cycle aging.

In different studies differential voltage analysis (dV/dQ or dV/dSOC) was used to identify degradation mechanism [4,10,32,33]. Peaks in a differential voltage curve result from phase transitions or staging phenomena. In Section 3.2.2 we assigned the peaks in Fig. 11 to transitions between voltage plateaus of the negative electrode using half-cell measurements. During aging different degradation processes can occur, either leading to a loss of active lithium in the system, or reducing the accessible active material of one of the electrodes. The loss of accessible active material results in a decrease in distance between transition peaks of the electrode in question in a dV/dSOC curve. Loss of active lithium on the other hand, keeps the distance between the peaks constant while shifts occur, but can lead to extinction of peaks in case the amount of active lithium is not sufficient anymore to reach the transition [32].

In Fig. 19 the results of a differential voltage analysis of a cell stored at 50 °C and 100% SOC are displayed, exemplarily for calendar aging. In Fig. 19a) charge and discharge curves with 0.25 C at different states of health are shown, whereas in Fig. 19b) the differential voltage of the discharge curves are depicted. The two transition peaks of graphite are clearly visible in all curves. The peaks in Fig. 19b) shift, but the distance between the peaks stays constant between 45% and 46%. Similar results have been found for the other calendar aging tests. Fig. 20 shows the result for a cell stored at 50 °C and 50% SOC. The finding indicates that the degradation of the stored cells is mainly due to loss of lithium, which can be attributed to side reaction and is probably due to film formation on one of the electrodes, or both.

To compare calendar and cycle aging, in Fig. 21 the results of a cell cycled with 1 C at 35 °C between 10% and 90% SOC are shown. In this case as well as in most other results from cycled cells both graphite voltage transition peaks vanish over cycling. As capacity fade and resistance increase of the cell is similar to the stored one in Fig. 19 the disappearance of the peaks cannot be due to loss of active lithium. Bloom et al. [32] picture the theory that increased solvent co-intercalation [34] during cycling leads to reduction of difference in lithium reactivity between two plateaus and therefore reduces the change in voltage during transition between the plateaus. Anyway, this theory was not proved by further experiment, which is why also further theories have to be discussed. Also

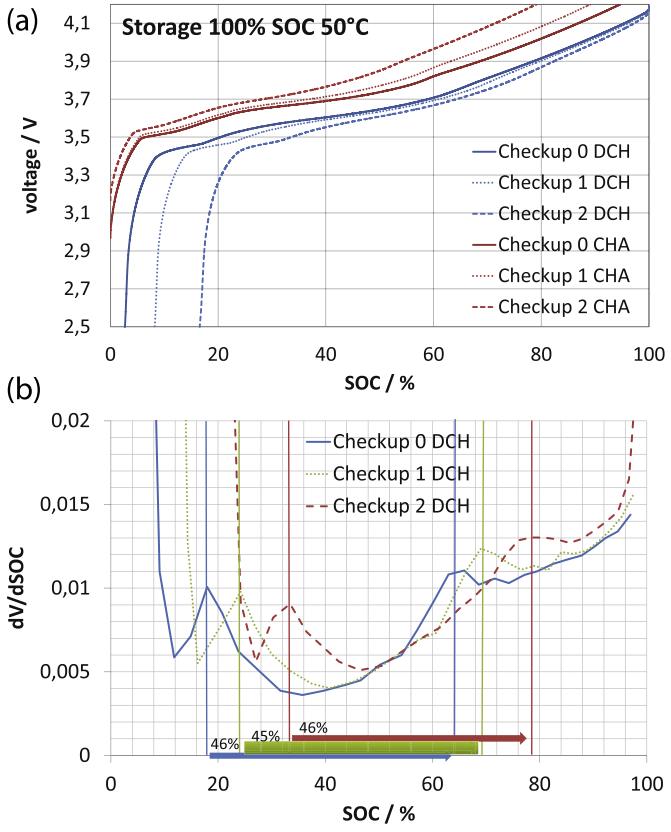

Fig. 19. Differential voltage analysis for cells stored at 50 °C and 100% SOC. (a) voltage vs. SOC. Charge (red) as well as a discharge curves (blue) with 0.25 C at 35 °C are shown for different checkup times. Checkup 2 is after 108 days of storage. Data of a single cell is shown. (b) differential voltage dV/dSOC vs. SOC for the discharge curves displayed in (a). (For interpretation of the references to color in this figure legend, the reader is referred to the web version of this article.)

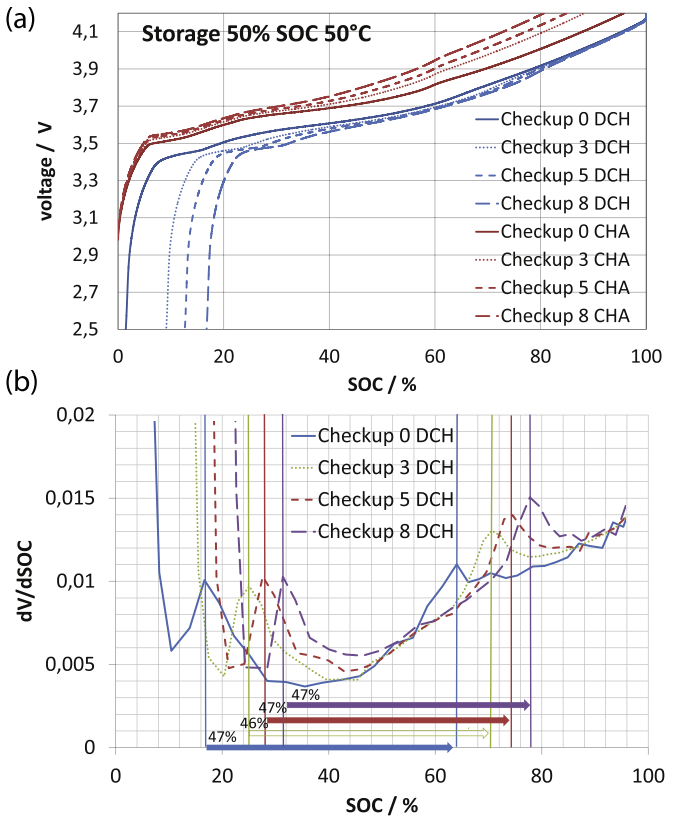

Fig. 20. Differential voltage analysis for cells stored at 50 °C and 50% SOC. (a) voltage vs. SOC. Charge (red) as well as a discharge curves (blue) with 0.25 C at 35 °C are shown for different checkup times. Checkup 8 is after 358 days of storage. Data of a single cell is shown. (b) Differential voltage dV/dSOC vs. SOC for the discharge curves displayed in (a). (For interpretation of the references to color in this figure legend, the reader is referred to the web version of this article.)

mechanical stresses during normal lithium de/intercalation can lead to disordering of graphite during cycling and smear the transition between plateaus. One could also imagine inhomogeneous load and therefore inhomogeneous degradation over the thickness of the electrode being the source to blur the voltage of a sharp transition. Physical simulations of lithium-ion cells revealed an inhomogeneous pore wall flux over electrode thickness, indicating such an inhomogeneous load [35,36]. Anyway, further work has to be done, especially analysis of the material changes, to illuminate the relation between calendar and cycle aging.

Fig. 22 displays the same analysis for a cell cycled in a graphite voltage plateau between 40% and 60% SOC. In this case the transition peak at around 64% SOC also vanishes over aging. But despite the similar loss of capacity of the two cycled cells, the peak at around 17% SOC of the cell cycled between 40% and 60% SOC diminishes, but does not vanish. In the case of cells cycled between 0% and 20% SOC, in contrast, having the same cycle depth, but do cross voltage transitions, the peaks vanish similar to the cell shown in Fig. 21. This leads to the conclusion that cells that do not cross any transition between voltage plateaus (see Section 3.3.1), are subject to less mechanical stress.

4. Conclusion

In this work, an extensive set of accelerated aging tests has been carried out employing a Li-ion high energy 18650 system (2.05 Ah, negative electrode: carbon, positive electrode: $Li(NiMnCo)O_2$). Different influence factors on calendar aging, such as temperature and voltage, as well as impact factors on cycle aging, like cycle depth and average SOC, have been investigated. The results can serve as a basis for the development of lifetime prediction models and inhere a better understanding of the aging process of lithium-ion batteries during cycling and storage. During lifetime, capacity loss, discharge resistances (after 2 s, 10 s and 17 s) and charging resistances (2 s, 10 s) at different SOC, impedance spectra and C/4 discharge voltage curves have been recorded. In this work the focus was on the evaluation of capacity, resistance and C/4 discharge voltage curves, the results obtained by impedance spectroscopy will be discussed in a separate paper. Analysis revealed that the different resistances under consideration showed the same aging behavior and the 17 s discharge resistance at 50% SOC has been chosen for degradation analysis.

During storage, aging proceeds with a linear dependency on time with only slight tendency to square root kind of evolution. Arrhenius behavior has been confirmed for the stored cells, with constant activation energy over lifetime. Storing cells at high SOC accelerated degradation; especially 100% SOC damages the cells most. The influence of voltage level on calendar aging has been found to correlate with the carbon potential. If such a correlation proves to be valid for other cell technologies, it could be an interesting correlation to implement voltage dependency in aging models.

Cycled cells have been found to die suddenly within only a few cycles after reaching a certain stage in lifetime. Cycle depth has a linear impact on aging, where deeper cycles accelerate aging. The

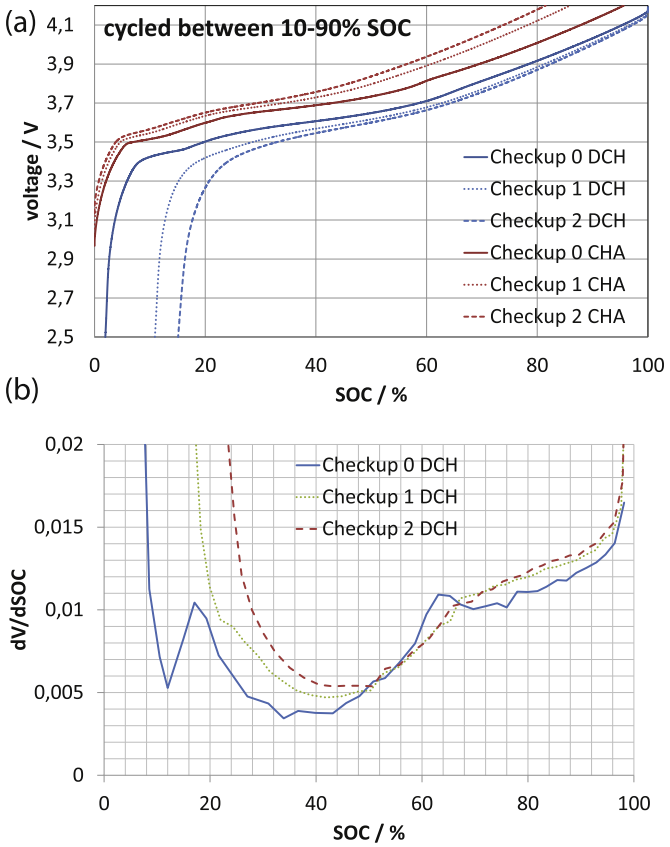

Fig. 21. Differential voltage analysis for cells cycled with 1 C at 35 °C between 10% and 90% SOC. (a) voltage vs. SOC. Charge (red) as well as a discharge curves (blue) with 0.25 C at 35 °C are shown for different checkup times. Checkup 2 is after 470 equivalent full cycles. Data of a single cell is shown. (b) Differential voltage dV/dSOC vs. SOC for the discharge curves displayed in (a). (For interpretation of the references to color in this figure legend, the reader is referred to the web version of this article.)

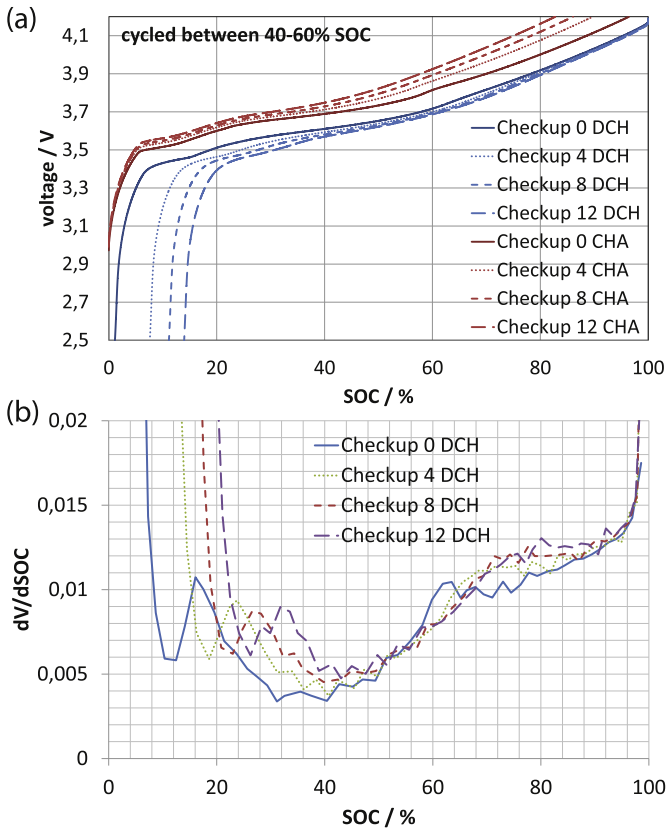

Fig. 22. Differential voltage analysis for cells cycled with 1 C at 35 °C between 40% and 60% SOC. (a) voltage vs. SOC. Charge (red) as well as a discharge curves (blue) with 0.25 C at 35 °C are shown for different checkup times. Checkup 12 is after 3053 equivalent full cycles. Data of a single cell is shown. (b) Differential voltage d*V*/dSOC vs. SOC for the discharge curves displayed in (a). (For interpretation of the references to color in this figure legend, the reader is referred to the web version of this article.)

average SOC during a cycle impacts aging in a way, that there is an optimum for cycles around 50% SOC, whereas cycles around lower and higher SOC accelerate degradation. The results indicate that cells crossing a transition between voltage plateaus of the carbon material during cycling show faster aging due to mechanical stresses. Comparison between calendar and cycle aging tests revealed, that cycling the battery adds additional degradation compared to storage considering capacity as well as resistance. Differential voltage analysis was used to identify the difference in aging mechanisms during storage and cycling. Especially cycling with cycles that cross transitions between voltage plateaus of the carbon seems to destroy the carbon structure in a way that transition peaks are not observed anymore in the C/4 discharge curve after significant aging. Anyway, to obtain a more profound understanding of the relation between calendar and cycle aging, more investigation, especially involving post-mortem analysis to identify the single degradation mechanisms becomes necessary. Such an investigation is planned to be done soon. Furthermore, the results shown in this work are based on measurement results of one battery technology (Sanyo UR18650E). Further technologies have to be investigated in order to obtain more general conclusions.

Further studies of the results of impedance spectroscopy during this test as well as the application of the results shown here in a lifetime prediction model will be presented in separate publications.

Acknowledgments

The basis of this work has been performed in the framework of the research initiative “e performance” funded by the German Federal Ministry for Education and Research. The work has been continued in the framework of the research initiative “HGF Energie Allianz” funded by Impuls- und Vernetzungsfond der Helmholtz-Gemeinschaft e.V. Responsibility for the content of this publication lies with the authors.

References

[1] M. Kassem, J. Bernard, R. Revel, S. Pélissier, F. Duclaud, C. Delacourt, J. Power Sources 208 (2012) 296–305.
[2] Q. Zhang, R.E. White, J. Power Sources 173 (2007) 990–997.
[3] J. Wang, P. Liu, J. Hicks-Garner, E. Sherman, S. Soukiazian, M. Verbrugge, H. Tataria, J. Musser, P. Finamore, J. Power Sources 196 (2011) 3942–3948.
[4] K. Kumaresan, Q. Guo, P. Ramadass, R.E. White, J. Power Sources 158 (2006) 679–688.
[5] G. Ning, B. Haran, B.N. Popov, J. Power Sources 117 (2003) 160–169.
[6] R.B. Wright, C.G. Motloch, J.R. Belt, J.P. Christophersen, C.D. Ho, R.A. Richardson, I. Bloom, S.A. Jones, V.S. Battaglia, G.L. Henriksen, T. Unkelhaeuser, D. Ingersoll, H.L. Case, S.A. Rogers, R.A. Sutula, J. Power Sources 110 (2002) 445–470.
[7] I. Bloom, B. Cole, J. Sohn, S. Jones, E. Polzin, V. Battaglia, G. Henriksen, C. Motloch, R. Richardson, T. Unkelhaeuser, D. Ingersoll, H. Case, J. Power Sources 101 (2001) 238–247.
[8] M. Ecker, J.B. Gerschler, J. Vogel, S. Käbitz, F. Hust, P. Dechent, D.U. Sauer, J. Power Sources 215 (2012) 248–257.
[9] S. Käbitz, J.B. Gerschler, M. Ecker, Y. Yurdagel, B. Emmermacher, D. André, T. Mitsch, D.U. Sauer, J. Power Sources 239 (2013) 572–583.
[10] I. Bloom, L.K. Walker, J.K. Basco, D.P. Abraham, J.P. Christophersen, C.D. Ho, J. Power Sources 195 (2010) 877–882.
[11] M. Dubarry, C. Truchot, B.Y. Liaw, K. Gering, S. Sazhin, D. Jamison, C. Michelbacher, J. Power Sources 196 (2011) 10336–10343.
[12] J. Belt, V. Utgikae, I. Bloom, J. Power Sources 196 (2011) 10213–10221.
[13] J.H. Ryu, J.W. Kim, Y.-E. Sung, S.M. Oh, Electrochem. Solid State Lett. 7 (2004) A306–A309.
[14] K. Rhodes, N. Dudney, E. Lars-Curzio, C. Daniel, J. Electrochem. Soc. 157 (2010) A1354–A1360.
[15] V.A. Sethuraman, N. Van Winkle, D.P. Abraham, A.F. Bower, P.R. Guduru, J. Power Sources 206 (2012) 334–342.
[16] M. Hahn, H. Buqa, P.W. Ruch, D. Goers, M.E. Spahr, J. Ufheil, P. Novák, R. Kötz, Electrochem. Solid State Lett. 11 (9) (2008) A151–A154.
[17] V.A. Sethuraman, L.J. Hardwick, V. Srinivasan, R. Kostecki, J. Power Sources 195 (2010) 3655–3660.
[18] R. Deshpande, Y. Cheng, M.W. Verbrugge, A. Timmons, J. Electrochem. Soc. 158 (6) (2011) A718–A724.
[19] K. Dokko, M. Nishizawa, S. Horikoshi, T. Itoh, M. Mohamedi, I. Uchida, Electrochem. Solid State Lett. 3 (3) (2000) 125–127.
[20] W. Waag, S. Käbitz, D.U. Sauer, Appl. Energy 102 (2013) 885–897.
[21] M. Broussely, S. Herreyre, P. Biensan, P. Kasztejna, K. Nechev, R.J. Staniewicz, J. Power Sources 97–98 (2001) 13–21.
[22] H.J. Ploehn, P. Ramadass, R.E. White, J. Electrochem. Soc. 151 (2004) A456–A462.
[23] K. Edström, T. Gustafsson, J.O. Thomas, Electrochim. Acta 50 (2004) 397–403.
[24] M. Broussely, P. Biensan, F. Bonhomme, P. Blanchard, S. Herreyre, K. Nechev, R.J. Staniewicz, J. Power Sources 146 (2005) 90–96.
[25] D. Aurbach, J. Power Sources 89 (2000) 206–218.
[26] R. Spotnitz, J. Power Sources 113 (2003) 72–80.
[27] B.Y. Liaw, E. Roth, R.G. Jungst, G. Nagasubramanian, H.L. Case, D.H. Doughty, J. Power Sources 119–121 (2003) 874–886.
[28] J.R. Dahn, Phys. Rev. B 44 (1991) 9170–9177.
[29] T. Ohzuku, Y. Iwakoshi, K. Sawai, J. Electrochem. Soc. 140 (9) (1993) 2490–2498.
[30] J.O. Besenhard, H.P. Fritz, Angew. Chem. Int. Ed. Engl. 22 (1983) 950–975.
[31] D.U. Sauer, H. Wenzl, J. Power Sources 176 (2008) 534–546.
[32] I. Bloom, J.P. Christophersen, D.P. Abraham, K.L. Gering, J. Power Sources 157 (2006) 537–542.
[33] J. Deshpande, M. Verbruggr, Y. Cheng, J. Wang, P. Liu, J. Electrochem. Soc. 159 (10) (2012) A1730–A1738.
[34] J.O. Besenhard, Carbon 14 (1976) 111–115.
[35] T.F. Fuller, M. Doyle, J. Newman, J. Electrochem. Soc. 141 (1) (1994) 1–10.
[36] M. Doyle, T.F. Fuller, J. Newman, J. Electrochem. Soc. 140 (6) (1993) 1526–1533.